REPORT DOCUMENTATION PAGE

Form Approved OMB No 0704-0188

AD-A274 971

2. REPORT DATE	3. REPORT TYPE AND DATES COVERED
August 14, 1993	Annual August 14, 1992-August 14, 1993

4. TITLE AND SUBTITLE
Low Threshold All-Optical Crossbar Switch on GaAs-GaA/As Channel Waveguide Arrays

5. FUNDING NUMBERS
c: F49620-92-C-0047

6. AUTHOR(S)
Tomasz Jannson, Ph.D.

AFOSR-TR- 94 0033

7. PERFORMING ORGANIZATION NAME(S) AND ADDRESS(ES)
Physical Optics Corporation
2545 West 237th Street
Torrance, CA 90505

8. PERFORMING ORGANIZATION REPORT NUMBER
3176

DTIC ELECTE JAN 27 1994 S C D

9. SPONSORING/MONITORING AGENCY NAME(S) AND ADDRESS(ES)
Contracting Officer
AFOSR/PK
Bolling AFB, DC 20332-6448

10. SPONSORING/MONITORING AGENCY REPORT NUMBER
1602/01

11. SUPPLEMENTARY NOTES

12a. DISTRIBUTION/AVAILABILITY STATEMENT
Distribution Unlimited

12b. DISTRIBUTION CODE

13. ABSTRACT *(Maximum 200 words)*

POC has proposed a 10 × 10 all-optical crossbar switch based on an optically activated modulator. A laser beam with an energy higher than the bandgap of the GaAs switches the propagation direction of the guided beam. Strong index modulation (>2%) can be induced by this method, which is not dependent on polarization for the EO effect. Both TE and TM guided waves have the same induced index change. Because there are no electrical contacts, this all-optical switch has no RC time limits. The switching speed is limited only by the generated carrier lifetime, which is in the picosecond range. Being the basic building block for high-speed optoelectronic computing and signal processing, this generic concept is applicable to a broad variety of photonic components, including optical logic gates, EO modulators, variable delay lines, and crossbar reconfigurable interconnects. To optimize the switching efficiency, several optical switch designs were studied, including cross switches and directional coupler switches. To realize the multichannel optical switches, a compact self-aligned packaging technique was developed. An all-optical switch using a 0.8 μm pumping laser beam and a 1.3 μm probe beam has been demonstrated, and efficiency as a function of pumping power and wavelength was studied.

14. SUBJECT TERMS
high speed modulation, GaAs switch, crossbar switch

15. NUMBER OF PAGES

16. PRICE CODE

17. SECURITY CLASSIFICATION OF REPORT	18. SECURITY CLASSIFICATION OF THIS PAGE	19. SECURITY CLASSIFICATION OF ABSTRACT	20. LIMITATION OF ABSTRACT
Unclassified	Unclassified	Unclassified	SAR

NSN 7540-01-280-5500

Standard Form 298 (Rev. 2-89)
Prescribed by ANSI Std. 239-18
298-102

94-02658

94 1 26 107

Research Sponsored by the Air Force Office of Scientific Research (AFMC)

Contract No.: F49620-92-C-0047

Low Threshold All-Optical Crossbar Switch on GaAs-GaAlAs Channel Waveguide Arrays

Annual Report

Submitted to:

Contracting Officer
AFOSR/PK
Bolling AFB, DC 20332-6448

Contractor:

Physical Optics Corporation
Applied Technology Division
2545 West 237th Street, Suite B
Torrance, CA 90505

Principal Investigator:

Tomasz Jannson, Ph.D.
(310) 530-1416

August 14, 1993

ABSTRACT

POC has proposed a 10 × 10 all-optical crossbar switch based on an optically activated modulator. A laser beam with an energy higher than the bandgap of the GaAs switches the propagation direction of the guided beam. Strong index modulation (>2%) can be induced by this method, which is not dependent on polarization for the EO effect. Both TE and TM guided waves have the same induced index change. Because there are no electrical contacts, this all-optical switch has no RC time limits. The switching speed is limited only by the generated carrier lifetime, which is in the picosecond range. Being the basic building block for high-speed optoelectronic computing and signal processing, this generic concept is applicable to a broad variety of photonic components, including optical logic gates, EO modulators, variable delay lines, and crossbar reconfigurable interconnects. To optimize the switching efficiency, several optical switch designs were studied, including cross switches and directional coupler switches. To realize the multichannel optical switches, a compact self-aligned packaging technique was developed. An all-optical switch using a 0.8 μm pumping laser beam and a 1.3 μm probe beam has been demonstrated, and efficiency as a function of pumping power and wavelength was studied.

TABLE OF CONTENTS

1.0 INTRODUCTION

In this Phase II project, POC proposed to build a low threshold 10×10 all-optical crossbar switch based on an optically activated modulator (OAM). The 10×10 crossbar switch is shown in Figure 1-1, where a laser beam with an energy higher than that of the bandgap of the GaAs semiconductor is used to optically switch the guided beam propagation direction, and thus the receiving ports. The optical switch is one of the major building blocks of optoelectronic integrated circuits (OEICs) for optical communications, because of its capability of providing optical signal processing. Because of the small index change induced by the electro-optic effect, most conventional EO waveguide switches have a long strip waveguide and large polarization dependence. Additionally, they suffer from large device dimensions and low packaging densities.

It has been shown in semiconductor lasers that a carrier induced index change can be two orders of magnitude larger than that produced by the EO effect. Based on this strong carrier induced index change, highly efficient and dense optical switches can be fabricated on a fully integrated optoelectronic circuit. Another important feature is that, in contrast to the EO effect (which depends on the vector electric field), the carrier induced index change is a scalar function that operated independent of the polarization state of the guided beam; i.e., the induced change in the guiding layer index is the same for both TE and TM guided waves.

In this Phase I program, Physical Optics Corporation (POC) proposed and then successfully demonstrated a miniaturized optically activated modulator (OAM) based on a GaAlAs/GaAs channel waveguide and waveguide array. A 5-μm activation window is used to input a ~mW HeNe 632.8 nm laser beam which, in turn, modulates the 1.3 μm guided light [1]. Modulation depths from 33% to 85% have been observed on the various devices tested. The size of the activation window is much smaller than for a linear electrooptic device (~mm to ~cm), and a high power laser was not used in this demonstration.

In this Phase II project, several different optical switch designs were studied, including cross-switches and directional-coupler switches. The modulation depths induced by different pumping wavelengths (0.7 μm - 0.8 μm) were also studied in order to optimize the efficiency of the device.

In order to realize the multi-channel optical switches, a compact self-aligned packaging technique was developed by POC during this program. The assembly architecture includes self alignment

and shrinkage-compensation soldering between single-mode fiber arrays and optical waveguide arrays.

The all-optical crossbar switch fabricated in this program can be used in both BMDO and civilian applications. These applications include high speed laser wavelength and incident direction sensors, GaAs-OAM-based IR countermeasure systems, low threshold all-optical crossbar switching devices, delay lines for phased array antennas, optical logic gates, data sampling and encoding, the generation of very short optical pulses, and time division multiplexing (TDM) and demultiplexing.

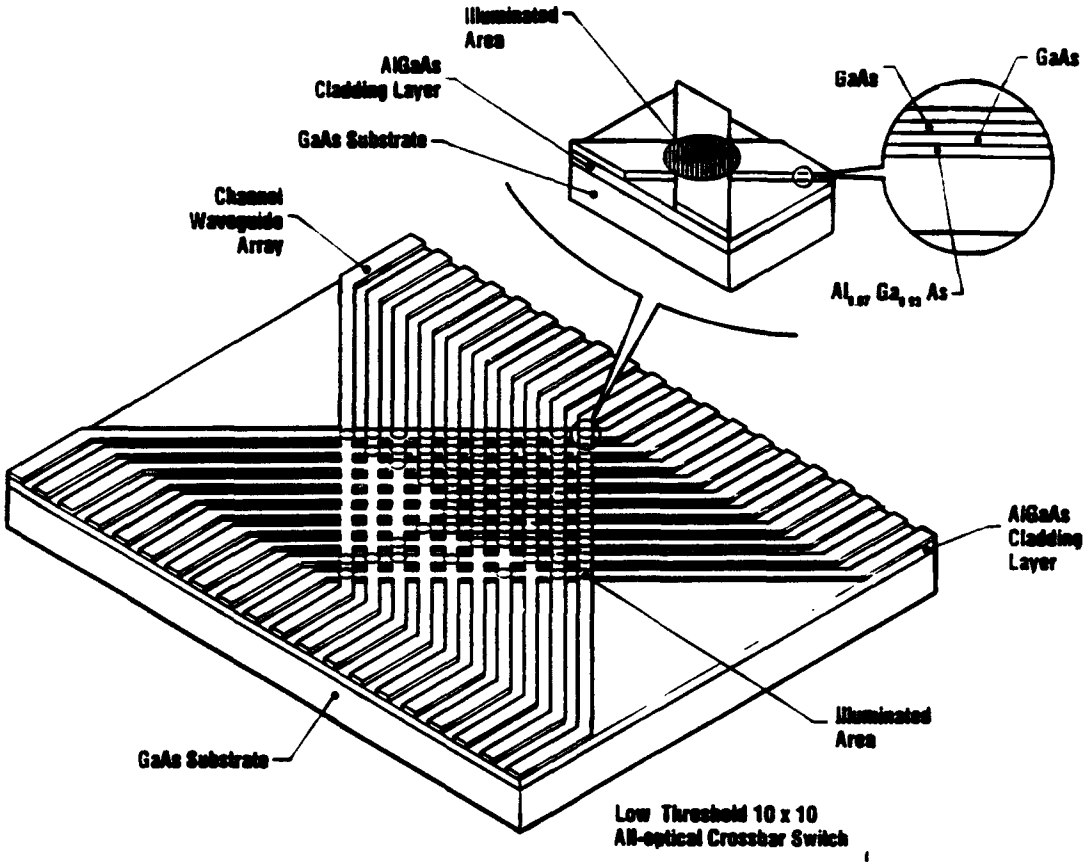

Figure 1-1
Low Threshold 10x10 All-Optical Crossbar Switch to be Demonstrated in Phase II

2.0 THE WORKING PRINCIPLE OF THE OPTICAL SWITCH

A discussion of the working principle of the modulator follows. A very large index change induced by current has been reported on Si [2,3], GaAs-GaAlAs [4], and InGaAsP-InP [5-7]. Since the current induced index change is much stronger than the linear electro-optic effect, we can make an active device by injecting a time dependent carrier concentration. The current is first induced by shining a strong condensed light with a photon energy larger than the band gap of the guiding layer material on the window area shown in Figure 1-1. In this way, a very large current density is induced. When the optical signal carrier to be modulated is coupled to the ridge waveguide, the induced current will interact with the guided wave.

The induced index change created by electron-hole pair generation can be written as

$$\Delta n = \frac{-2\pi N_e e^2}{m_e^* \omega^2 n_o} + \frac{-2\pi N_p e^2}{m_p^* \omega^2 n_o} \qquad (2\text{-}1)$$

where N_e and N_p represent the concentration of electrons and holes, respectively. By using the Kramers-Kronig relations, the absorption associated with free electrons and free holes is:

$$\Delta\alpha = \left(e^3\lambda^2 / 4\pi^2 C^3 \varepsilon_o n_o\right)\left[N_e / m_o^{*2}\mu_e + N_h / m_p^{*2}\mu_p\right] \qquad (2\text{-}2)$$

where e is the electron charge, ε_o is the permittivity of free space, μ_e is the electron mobility, and μ_p is the hole mobility. With an interaction length of 5 μm, the throughput intensity modulation is caused mainly by refractive index modulation (Eq. (2-1)), rather than absorption (Eq. (2-2)). It was proven in this program that the change of index of refraction due to the injected free carriers can be two orders of magnitude higher than that generated by the linear electrooptic (EO) effect. A device interaction length that is compatible with a multi-quantum well structure is achievable using this proposed concept.

Another important conclusion from Eq. (2-1) is that, in contrast to the linear electro-optic effect (which depends upon the vector electric field), the induced index change is a scalar function. If the effective masses of electrons and holes in the two different transverse directions are the same, then the induced change of the guiding layer index is the same for both TE and TM guided waves. This eases the requirement needed for the direction of waveguide propagation.

3.0 DESIGN, FABRICATION AND PACKAGING

3.1 Channel Waveguide Design

From the experimental point of view, the key point of optimization of a single-mode channel waveguide at a given wavelength is the accuracy involved in determining the ΔN value at the wavelength of interest. In order to achieve the required accuracy, it is necessary to first theoretically determine the proper waveguide parameters, such as waveguide width and depth. The challenge here is to precisely determine the effective index of the guided mode at the desired optical wavelengths under various waveguide dimensions and cladding layer indices. Marcatili's method [16] is used to determine the upper boundary of the waveguide cut-off dimensions at 1.3 μm and 1.5 μm with Al concentrations equal to 5% and 7%. The results are displayed in Figures 3-1 and 3-2.

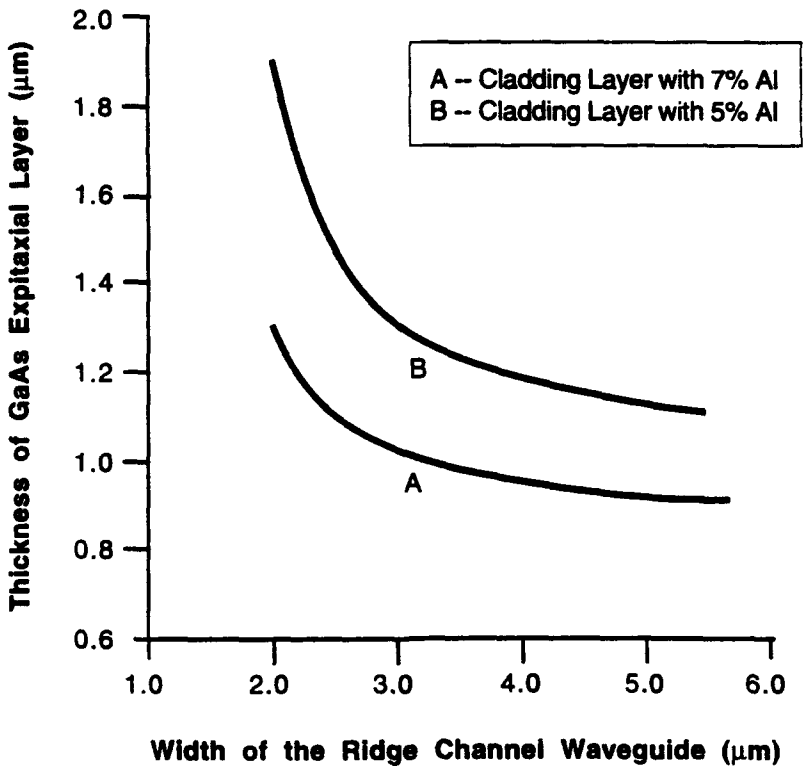

Figure 3-1
The Calculated Results of Cutoff Dimension on GaAs-GaAlAs Heterostructure Ridge Channel Waveguide with Al = 5% and 7% at 1.3 μm Wavelength

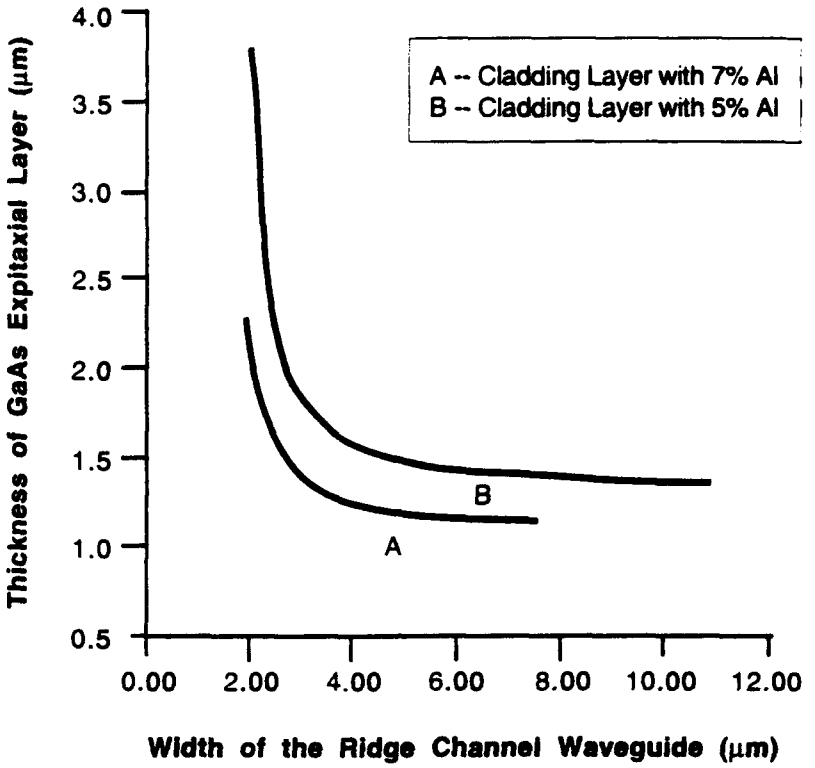

Figure 3-2
The Calculated Results of Cutoff Dimension on GaAs-GaAlAs Heterostructure Ridge Channel Waveguide with Al = 5% and 7% at 1.55 μm Wavelength

3.2 Material Design

The optical switch is grown on the GaAs substrate using the most advanced Metal Organic Chemical Vapor Deposition (MOCVD) technique. The material structures are shown in Figure 3-3. First, the cladding layer ($Al_{0.07}$ $Ga_{0.93}$) with a thickness of 1.5 μm is grown on the n^+ GaAs buffer layer. Then, a 4 μm undoped GaAs layer is grown as the guiding layer, which has a background doping under 10^{14} cm^{-3}. Then, the p^+ type base layer is grown, which is heavily doped to 10^{19} cm^{-3}. Above the base layer, an n type $Al_{0.25}Ga_{0.75}$ layer (to be used as the emitter) is grown with a doping density of 5×10^{17} cm^{-3} and a thickness of 2000Å . Finally, the n^+ GaAs capping layer is grown on the top. The material structures are verified by the polaron doping profiler. The measured thicknesses and doping concentrations are shown in Figure 3-4 . The emitter and base doping densities are close to the specified values.

Ohmic Contact	2000 Å	N^+ GaAs	1×10^{18} cm^{-3}
Emitter	2000 Å	N^+ $A\ell_{0.25}Ga_{0.75}As$	5×10^{18} cm^{-3}
Photosensitive Base	1500 Å	p GaAs	1×10^{18} cm^{-3}
Guiding Layer	40000 Å	i GaAs	1×10^{14} cm^{-3}
Cladding Layer	15000 Å	i $A\ell_{0.07}Ga_{0.95}As$	1×10^{14} cm^{-3}
Collector and Substrate	10000 Å	n^+ GaAs	1×10^{18} cm^{-3}

Figure 3-3
Epilayer Structure of the Multilayer Optical Switch

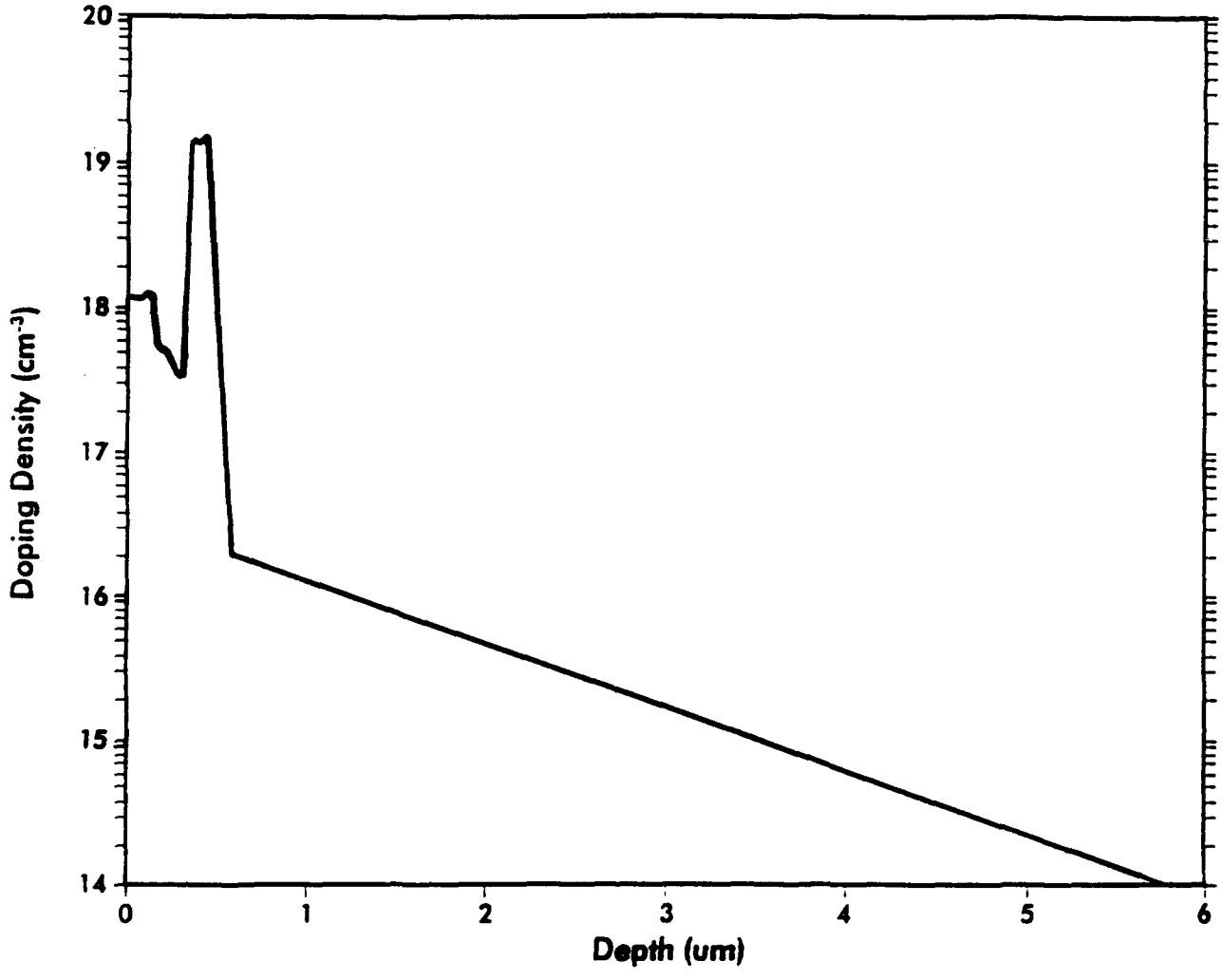

Figure 3-4
Carrier Doping Density Inside the Optical Switch Structure

3.3 Device Packaging

In the area of packaging, POC has developed a new assembly architecture for the alignment of and the soldering between single-mode fiber arrays and optical waveguide arrays, as shown in Figure 3-5. The assembly architecture has two key processes for optical coupling between the single-mode fiber arrays and the optical waveguide arrays, namely, alignment and fixing. Each process requires sub-μm precision, and typically has the following problems. First, the alignment between the arrays is very complicated, because their positions have six degrees of freedom, particularly, rotational degrees of freedom, which makes alignment more difficult. Soldering, which is typically used for fixing, can cause misalignments due to thermal shrinkage of the assembly equipment and solder volume. In order to solve these problems, an image position detection method is used to eliminate degrees of freedom for alignment. This allows the assembly throughput to be much better than that of conventional assembly architectures. Also, the use of a thermal shrinkage compensation method achieves high-precision soldering by canceling misalignments caused by the thermal shrinkage of assembly equipment and solder volume.

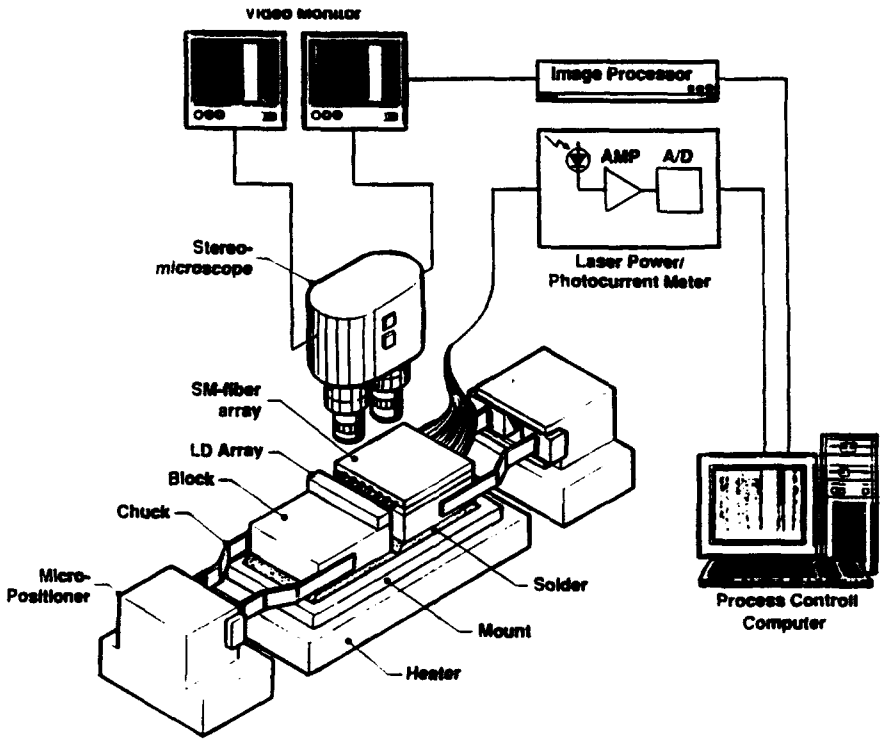

Figure 3-5
Illustration of Fiber/Waveguide Array Coupling System, for Coupling Between Fiber Ribbon (from Both Sides) and Integrated Optical Circuit

3.4 Single-Mode Fiber Array

A schematic view of the single-mode fiber array is shown in Figure 3-6. The single-mode fiber array is sandwiched and soldered between two V-grooved silicon substrates.

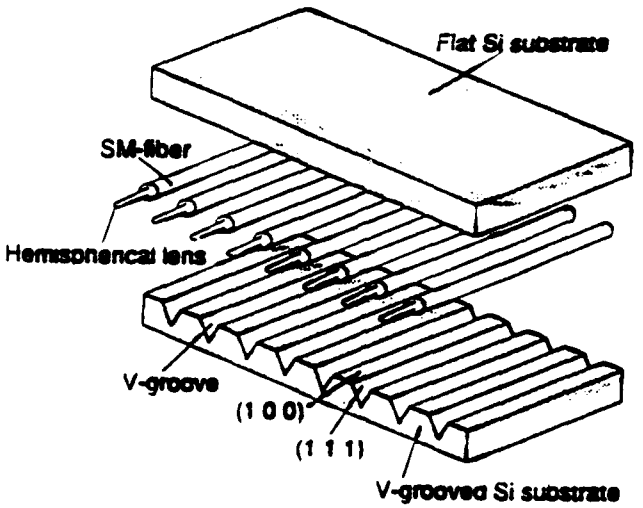

Figure 3-6
Schematic View of the SM-Fiber Array

The single-mode fiber has a 10-μm diameter core and a 125 μm diameter cladding. The V-grooves are formed on a silicon substrate through anisotropic etching using a KOH solution. They are designed to have 250 μm intervals and 160 μm depths. With careful silicon crystal orientation and control of the etching environment, the fiber arrangement can achieve ±0.5 μm precision.

Hemispherical lenses are formed at the fiber-ends in order to improve the optical coupling efficiency between the single-mode fiber array and the optical waveguide arrays. The lens formation process is shown in Figure 3-7. The fiber-ends are etched simultaneously using an HF solution, and then melted using an electric discharger. In pre-assembly, the single-mode fiber array is soldered onto the metal block.

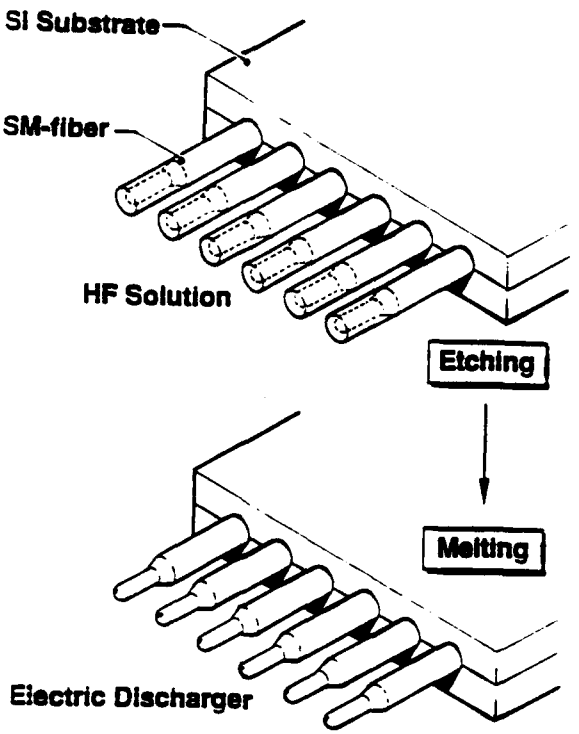

Figure 3-7
Hemispherical Lens Formation Process

3.5 Optical Coupling

In order to provide optical coupling with a maximum excess loss of 2 dB between the single-mode fiber array and the channel waveguide array requires a ± 1.5 μm precision. This precision must be achieved throughout the entire process: fiber arrangement, channel waveguide bending, alignment, and soldering. Each process, except for alignment, requires ± 0.5 μm precision. The coupling efficiency is remarkably changed by lateral misalignment of the X and Y axes, which are, respectively, parallel and vertical to the channel waveguide array. The efficiency change for the Z-axis is 10 times less remarkable than for the other axes.

3.6 Alignment

The alignment between the single-mode fiber array and the channel waveguide array is usually performed for six degrees of freedom: X, Y, Z (the linear axes), and θx, θy and θz (the rotational

axes). Unfortunately, the alignment of the rotational axes interferes with the other axes, making the entire alignment procedure very time consuming. However, in POC's new architecture, the alignment for the Z, θ_x, and θ_y axes is simplified, because a larger tolerance is allowed for these three axes.

In presetting before alignment, the single-mode fiber array block and the channel waveguide array are held by chucks, and the mount is set on a heater, as shown in Figure 3-8. The blocks can be independently moved for alignment. The blocks and chucks are precisely manufactured in order to eliminate the alignment for the θ_x axis.

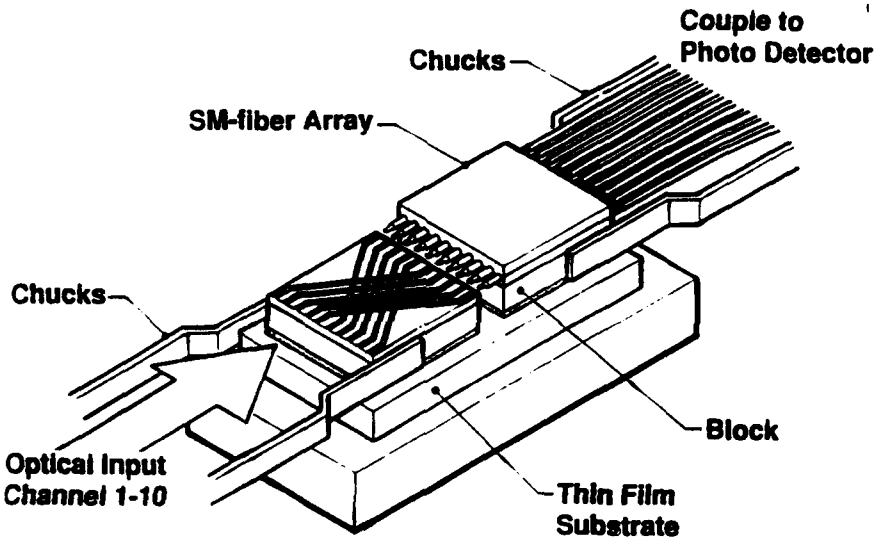

Figure 3-8
Soldering Process with the Thermal Shrinkage Compensation Method

The alignment process developed during this program is shown in Figure 3-9. In the process, rough alignment is performed prior to precise alignment in order to improve alignment throughout. The rough alignment achieves a $\pm$ 3 μm precision, which is sufficient for the Z and θy axes. The precision alignment uses the conventional active alignment method. By scanning the single-mode fiber array on the XY plane, the laser power meter measures the coupled laser power of the first and the last fibers. A 10 x 10 μm^2 area with a 0.5 μm interval is scanned. Misalignment for the X, Y and θz axes is corrected for using the (X,Y) position of the maximum laser power and the distance between the first and last channels. Thus, the array positions are correctly aligned without misalignments.

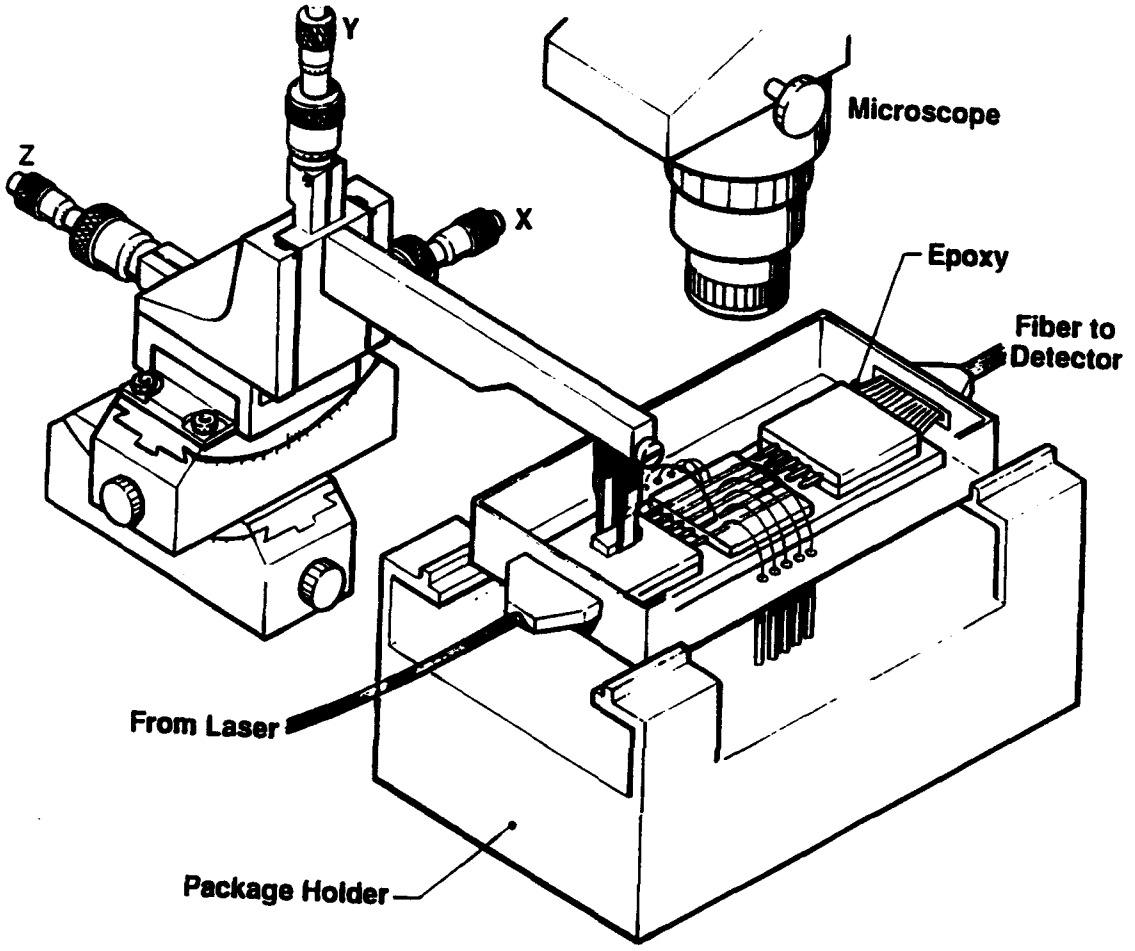

Figure 3-9
Schematic Diagram of the Assembly Equipment

3.7 Soldering

Soldering causes thermal shrinkage of the assembly equipment and the solder volume upon solidification. This is usually unavoidable. If the equipment has a 1m length, a thermal expansion coefficient of 10^{-6}/°C, and a temperature shift of 100°C, there will be a μm order misalignment, which leads to unsuccessful assembly. This misalignment can be canceled in POC's new assembly architecture.

The soldering process developed by POC is shown in Figure 3-8. It uses a new thermal shrinkage compensation method. The point of this method is that the single-mode fiber array block and channel waveguide array block are each held by two pairs of chucks having symmetrical structures and a low thermal expansion coefficient. Further, the chucks and micropositioners are adiabatic from the heater. In the soldering process, two solder layers between the two blocks and the mount are fused by the heater. Thermal shrinkage of the two chuck pairs and the two solder layers arises symmetrically. For the X, Y, θx, θy and θz axes, misalignment on the side of the single-mode fiber array is compensated for by misalignment on the side of channel waveguide array. In this, the single-mode fiber array block and the channel waveguide array block are soldered to a common mount with minimal misalignment.

After soldering, the assembled mount is fixed to the package using solder with a lower melting point. Finally, the package and the cap are hermetically solder-sealed. Because the assembly is performed before sealing the package, no work space is necessary inside the module. Therefore, the module can be made compact and narrow. This compact size is suitable for the use of a large number of modules in a real system. Assembly without adhesives has allowed the modules to have higher reliability at high temperatures.

4.0 MEASUREMENTS AND DISCUSSION

4.1 All-Optical Modulation Setup

A single-mode (8.7 μm core diameter) optical fiber was used to couple a 2.5 mW 1.3 μm laser beam into the GaAs optical switch, as shown in Figures 4-1 and 4-2.

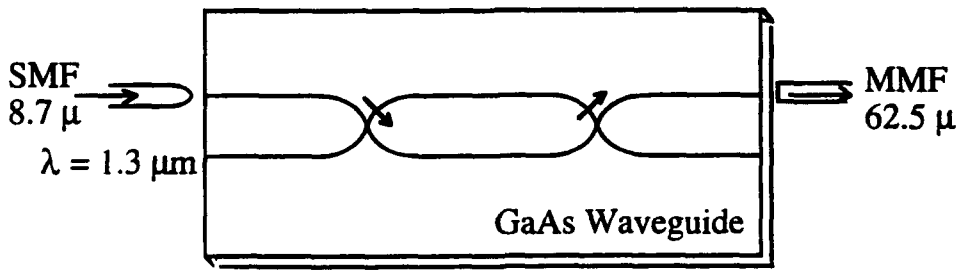

Figure 4-1
8.7 μm Core-Diameter Fiber was Used to Couple 1.3 μm Laser Beam From Semiconductor Laser into the GaAs Optical Switch. At the end of the waveguide, a 62.5 μm core-diameter fiber was used to couple out the laser beam.

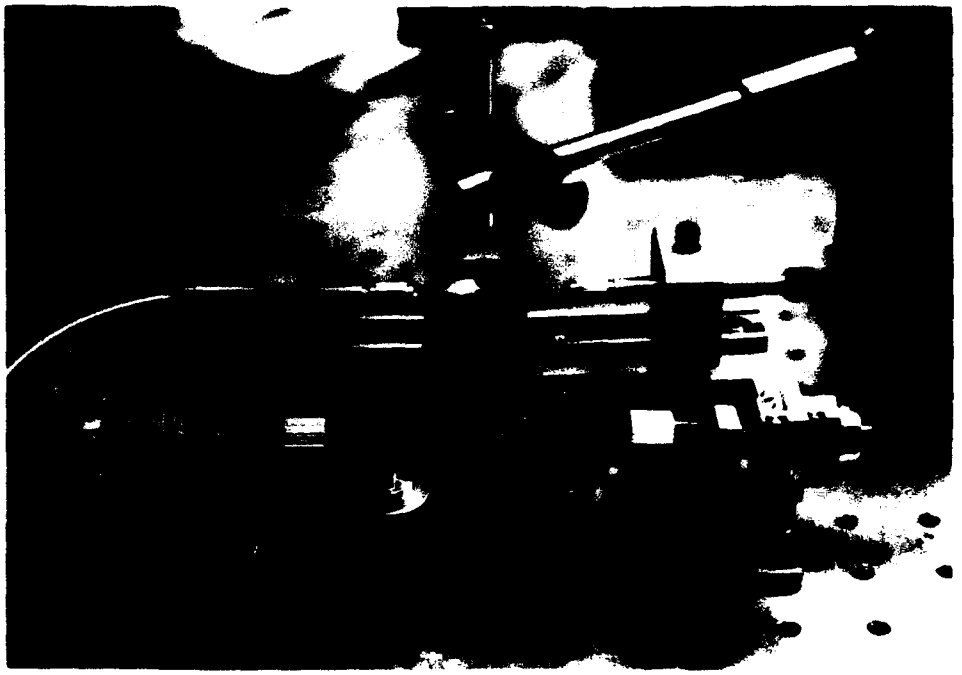

Figure 4-2
1.3 μm Laser Beam was Coupled into the Optical Switch from the Left-Hand-Side Single-Mode Fiber. The switched laser beam was then collected by a multi-mode fiber from the right-hand side. The pumping beam illuminates the X switch from the top.

The output light from the optical switch was then collected by a 62.5 μm multi-mode fiber. The optical switch was controlled by a laser beam from a Ti:Sapphire laser with an energy higher than the GaAs bandgap. A single-mode fiber was used to couple the laser beam from the Ti:Sapphire laser to the switch. The laser beam illuminated the intersection of the optical switch from the top, as shown in Figure 4-3. In order to observe significant optical switching, the pumping power from the Ti:Sapphire laser should be high. However, if the pumping power is too high, the heating effect will degrade the performance.

The complete setup of the all-optical switch is shown in Figures 4-4 and 4-5.

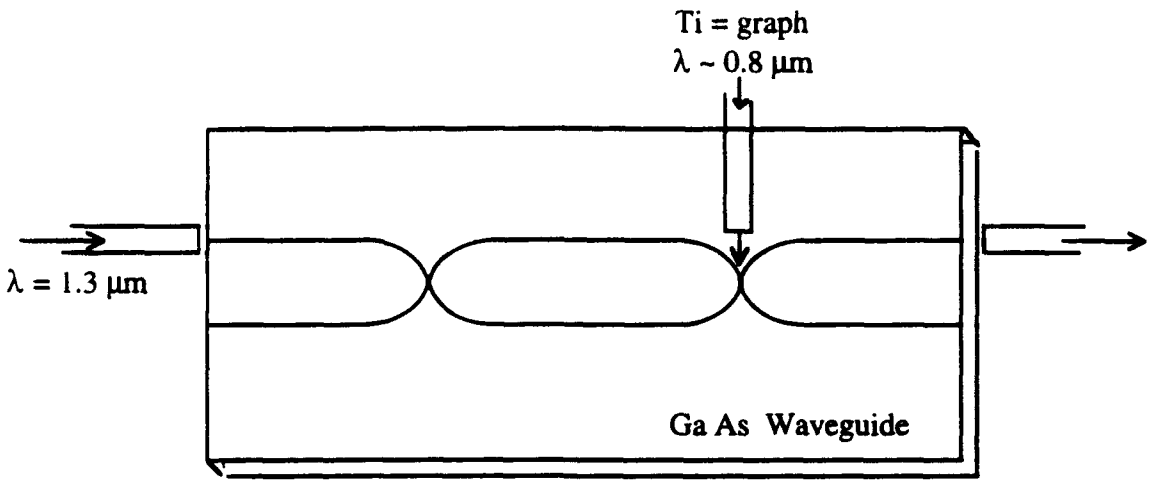

Figure 4-3
Tunable Laser Beam from Ti:Sapphire Laser was Used to Control the 1.3 μm Beam Switching. The pumping light energy must be higher than the GaAs bandgap energy.

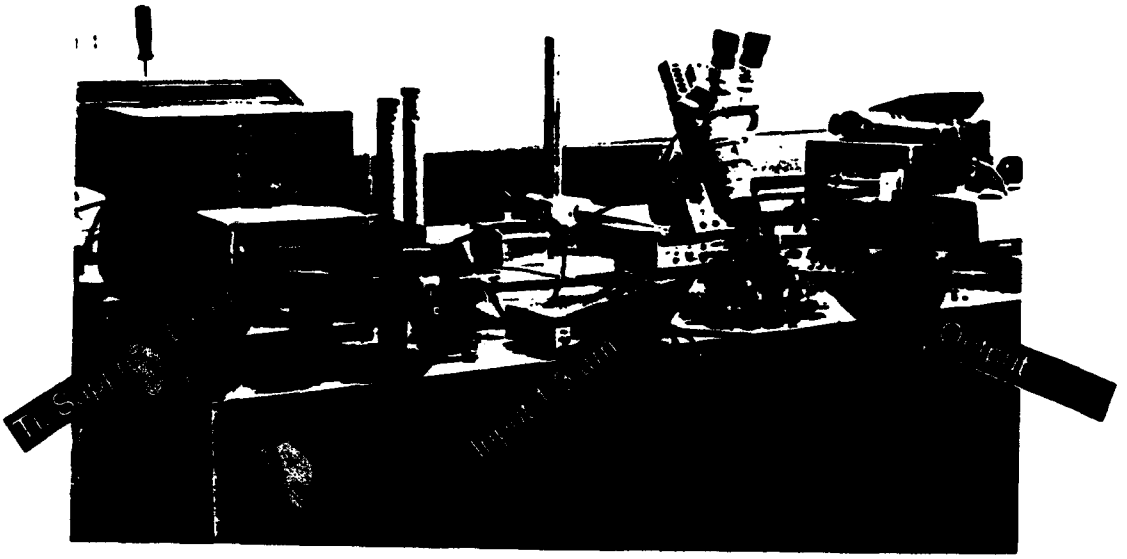

Figure 4-4
Photograph Showing the All-Optical X-Switch Measurement Setup

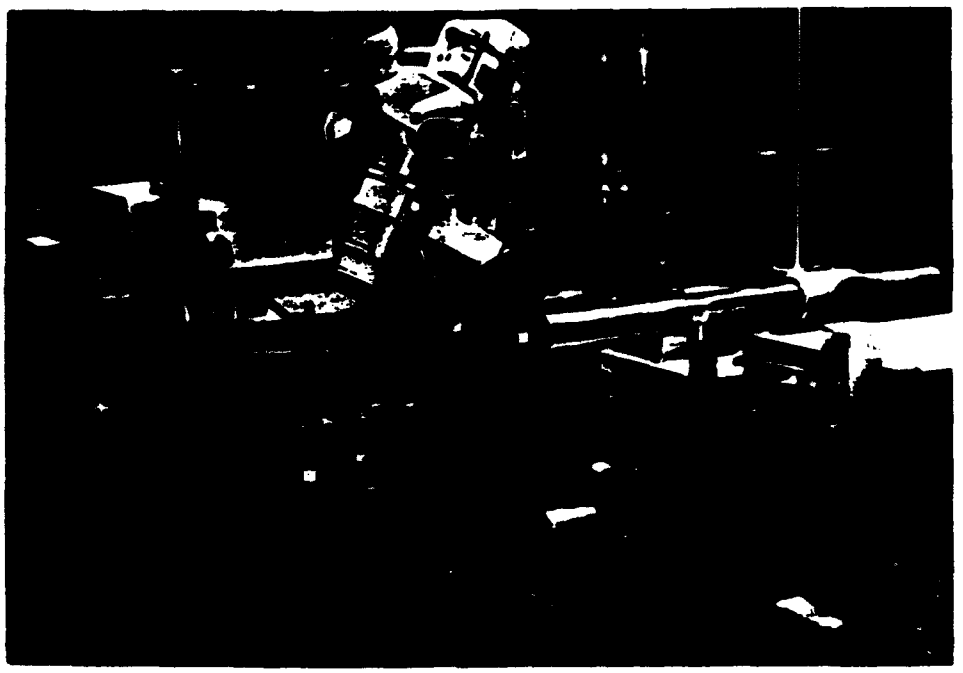

Figure 4-5
Pumping Light is $\lambda = 0.78$ μm From Ti:Sapphire Laser

4.2 All-Optical Switch Fabrication

The epistructure of the all-optical switch was grown using the MOCVD method on a GaAs substrate. A 1.5 μm thick undoped $Al_{0.07}Ga_{0.93}As$ cladding layer was first grown on the substrate. Then, a 4 μm undoped GaAs layer was grown on the top as a guiding layer. Conventional photolithography techniques were used to pattern the single-mode optical switches, as shown in Figure 4-6.

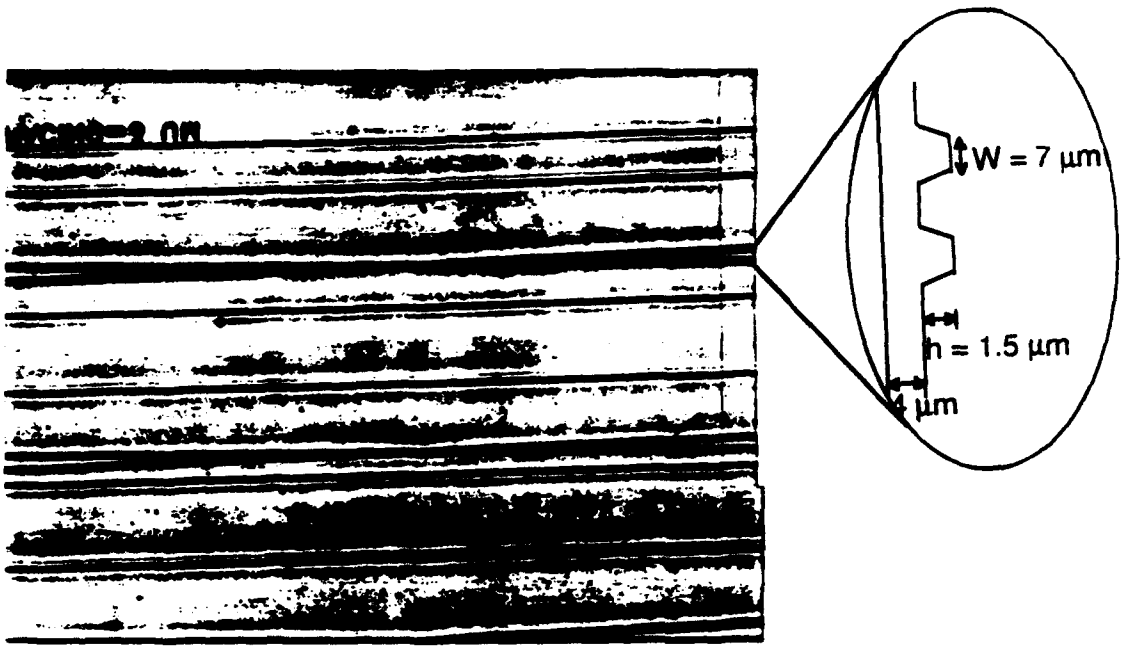

Figure 4-6
Photograph Showing the All-Optical X Switches. The width of the waveguide is 7 μm. The step height is h = 1.5 μm. The guiding layer is 4 μm thick. The pumping beam (λ = 0.78 μm) only illuminates the intersection areas.

4.3 All-Optical Switching Results

The switched laser beam was monitored by two InGaAs PIN detectors. The switched beams were first coupled to the single-mode fibers, and were then detected by the detectors, as shown in Figure 4-7.

The measured responses from the two arms of the X-switch are shown in Figure 4-8. When the pump light was on, the 1.3 μm guided beam was switched to arm (out 1). When it was turned off, the probe beam is switched back to arm (out 2). These results can be observed from the 180° phase change shown on the oscilloscope.

The absorption depth of the pumping light is a function of wavelength. It is well known that higher energy laser beams have shorter penetration depths. But, if the laser beam energy is lower than the GaAs bandgap, no switching will be observed. In order to observe this effect, the Ti:Sapphire laser was tuned from 700 nm to 900 nm. It was seen (see Figure 4-9) that when the pump light energy was below the GaAs bandgap, the modulation depth dropped dramatically. At

shorter wavelength ranges, the modulation depth dropped slowly, due to the reduced absorption depth.

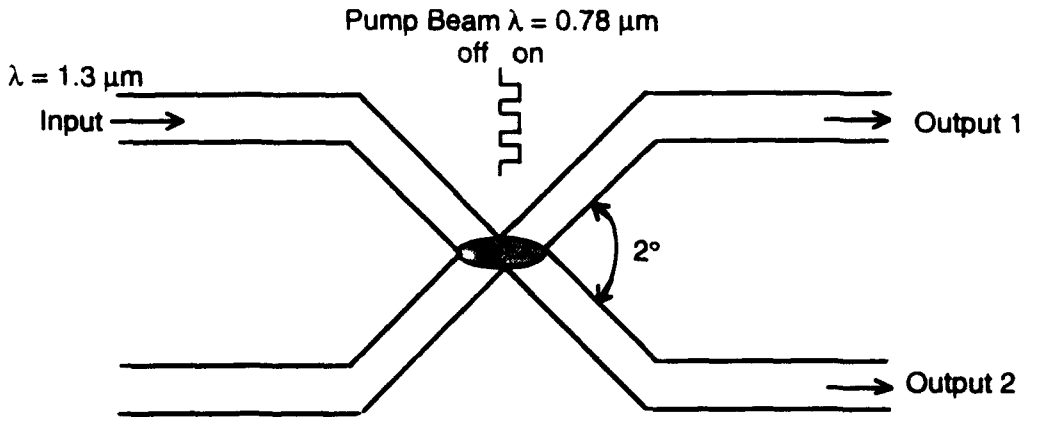

Figure 4-7
Output Signals From Different Arms of the X-Switch were Coupled to the Single-Mode Fibers and Monitored by Two InGaAs PIN Detectors

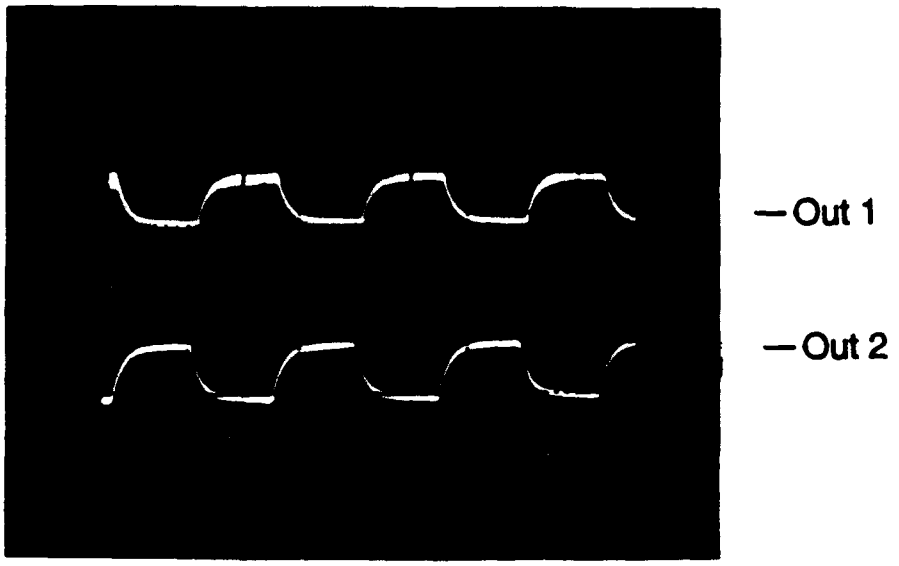

Figure 4-8
Output Signals From Different Arms of the X-Switch. When the pump beam is on, probe beam is switched to arm (out 1). When it is off, the probe beam is switched back to arm (out 2) again.

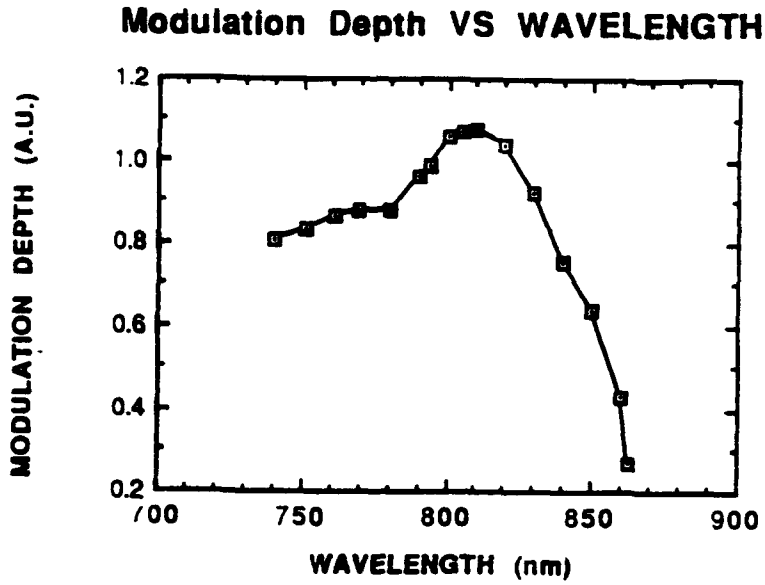

Figure 4-9
Modulation Depth as a Function of Pumping Wavelength. Modulation depth drop dramatically, when the pumping light energy is below the GaAs band gap. Modulation depth drop slowly at short wavelength range, due to the reduced absorption depth.

5.0 FUTURE DESIGNS USING BANDGAP ENGINEERING TECHNIQUES

5.1 Optical Switch with Quantum Well Devices

The speed of an all-optical switch with a bulk-type guiding layer is normally limited by the carrier relaxation time, which is typically longer than a nanosecond. In order to enhance the speed and efficiency of these devices, quantum well devices are implemented for high speed applications. Two different quantum well devices that have the necessary large current controllability and high speed performance are discussed in the following sections. The first is a heterojunction bipolar phototransistor (HBPT) device, while the other is a resonant tunneling double barrier device.

5.1.1 Heterojunction Bipolar Phototransistor (HBPT) Optical Switch

POC's HPBT optical switch, shown in Figure 5-1, has the unique high speed and high sensitivity properties for optoelectronic applications. Recently, a current gain of 50,000 was demonstrated

for a heterojunction bipolar phototransistor, inducing a photosensitivity of 15,000 A/W. Optical switches with HPBT structures have the following advantages:

- ultrahigh speed (~ picosecond)
- ultrahigh sensitivity
- integration capability with other OEICs
- high current gain

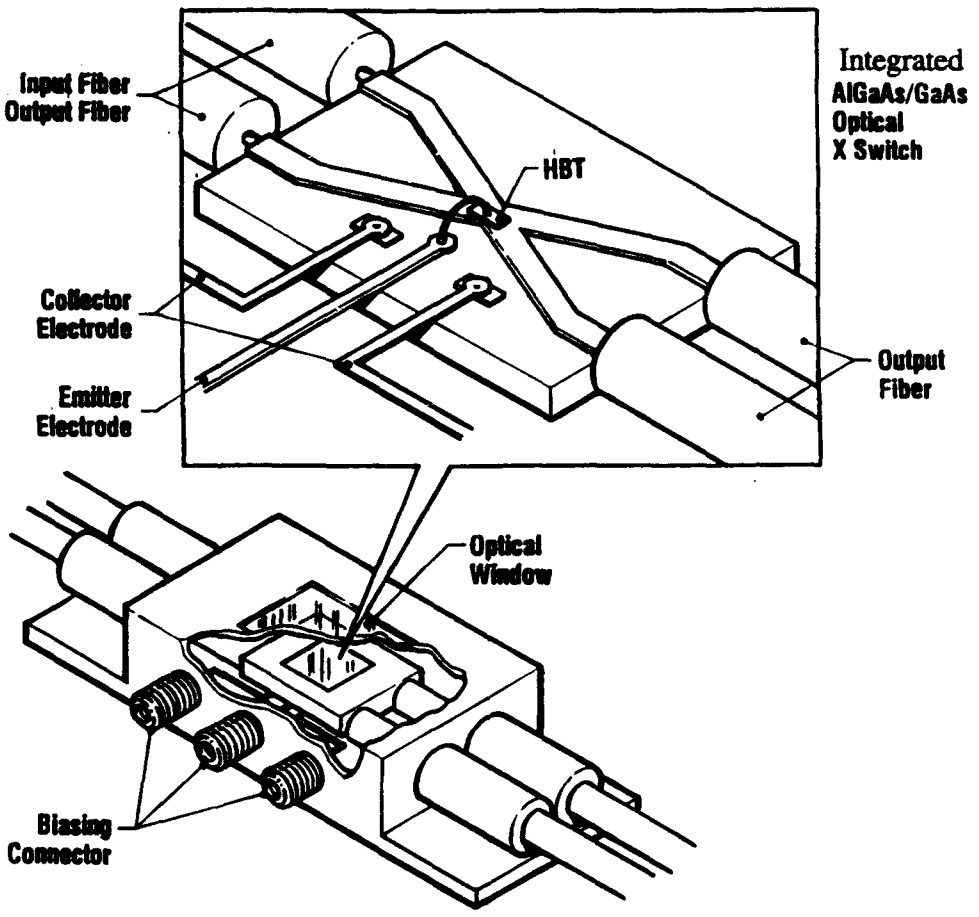

Figure 5-1
POC's High Speed, High Sensitivity All-Optical Switch HBPT Structures

The phototransistor action is achieved through the large emitter-collector current I_{EC}, which is controlled by a small base bias voltage V_{BE}. V_{BE} can be induced by electron-hole pair generation

inside the emitter-base and base-collector junctions. This mechanism can be utilized for a high speed phototransistor with an ultrahigh current gain, which can be controlled by a weak optical power. Due to the wide bandgap inside the emitter, a "window effect" can be achieved to enhance the device sensitivity. Due to the base energy barrier, most of the emitter current will be blocked by the barrier. When the base barrier is lowered by either electrical or optical means, the large emitter current is then injected into the collector (the guiding layer).

In an HPBT optical switch, only electrons are injected from the emitter into the collector guiding layer, which is not the same as the bulk-type guiding layer that has both electrons and holes generated inside the layer. So, the induced index change, Δn, is expressed as

$$\Delta n = \frac{-2\lambda \Delta N e^2}{m^* n_0 \omega^2} \tag{5-1}$$

where m^* is the effective mass of an electron, ω is the frequency, e is the electron charge, n_0 is the intrinsic index of refraction, and ΔN is the injected carrier density.

Several types of optical modulators and switches with p-n junctions whose operations are based on the applications of this phenomenon have been reported. However, the switching time of such diode-structure optical switches is most often limited by the injected carrier life time, which, in GaAs, is on the order of 10^{-8} s. Due to their high speed and high transconductance characteristics, HBTs are frequently applied in practical transistor circuits for high speed current switching. If a bipolar transistor structure is employed with the carrier injected into the base by optical injection, high speed optical switches and modulators may be achieved. The amplification nature of transistors also means that larger emitter or collector switching currents can be controlled either electrically or optically.

The approximate expressions for the rise time from 0% to 90%, t_r, and the fall time from 100% to 10%, t_f, for the output current when the transistor is driven by a constant input current in the common-based mode are given, respectively,

$$t_r = \left(\frac{1}{\omega_N} + M \alpha_N C_{ct} R_L \right) \ln \left(\frac{I_{E1}}{I_{E1} - \frac{0.9\, I_{Con}}{\alpha_N}} \right) \tag{5-2a}$$

$$t_f = \left(\frac{1}{\omega_N} + M' \alpha_N C_{ct} R_L \right) \ln \left(\frac{I_{Con} + \alpha_N I_{E2}}{0.1 I_{Con} + \alpha_N I_{E2}} \right) \qquad (5\text{-}2b)$$

where I_{E1} and I_{E2} are the values of the emitter current after the turn-on and turn-off steps are applied and α_N and ω_N are the normal small-signal current gain and cut-off frequency, respectively. I_{Con} is the collector current in the on-state, C_{ct} is the depletion layer capacitance, R_L is the load resistance, and M and M' are the functions of the collector-base voltages and the diffusion potential difference between the collector and base, respectively. The switching times as a function of the input emitter current are shown in Figure 5-2.

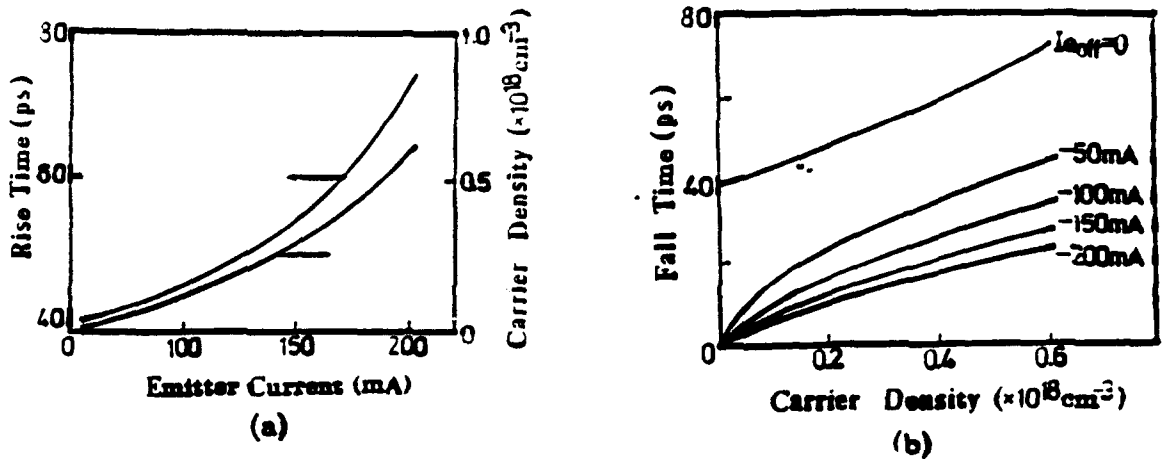

Figure 5-2
Calculated Switching Times of the Transistor: (a) Rise Time t_r and (b) Fall Time t_f

Note that both the rise time and the fall time will be around 50 ps for optical switching. Furthermore, POC's HB phototransistor benefits from the emitter "window effect", which makes it possible to illuminate the active zone through the wide band-gap emitter without the need for over dimensioning of the lateral zone. This is significant, because overdimensioning will sacrifice frequency performance. The other advantage of implementing the HB phototransistor structure within an optical device is the high current gain, which increases the sensitivity of the device and leads to a reduction in the surface area that needs to be illuminated.

5.1.2 Resonant Tunneling Double Barrier Quantum Well Optical Switch

The tunnel diode was named after Esaki, who first discovered it in 1958 [9]. The tunneling phenomenon is a majority carrier effect. Its response time is not limited by the minority carrier recombination lifetime (slow). The tunneling time of carriers through the potential energy barrier is not governed by the conventional transit time concept, but rather by the quantum transition probability per unit of time. This tunneling time is very short, permitting the use of tunnel devices well into the millimeter-wave region [10].

The applications for resonant tunneling diodes, including bistable operation [11], are all based on the negative differential resistance (NDR) in the current-voltage characteristic of the device, as shown in Figure 5-3. Furthermore, the use of a quantum well to form the double barrier structure means better control of the tunneling and the confinement of energy levels at room temperature [12]. The current voltage characteristics of a double barrier resonant tunneling diode shown in Figure 5-3, focuses on the negative differential resistance region. The peak current is primarily determined by the number of electrons passing through the resonant level. Thus, the magnitude of the peak current is influenced by the width of the resonant level. The valley current is the sum of the current contributions, such as non-resonant tunneling, tunneling through excited states in the quantum well, thermionic emission over the barriers, scattering assisted tunneling processes and leakage currents through surface states.

A resonant tunneling diode with a peak current density over 2×10^5 A/cm^2 has been demonstrated [13]. The higher the peak current, the more efficient the modulator/switch will be. Bistable operations of LED's and quantum well semiconductor lasers [14] have already been demonstrated by the integration of a resonant tunneling diode within the device structure. The waveguide modulator/switch will be the next target for state-of-the-art research in integrated optics.

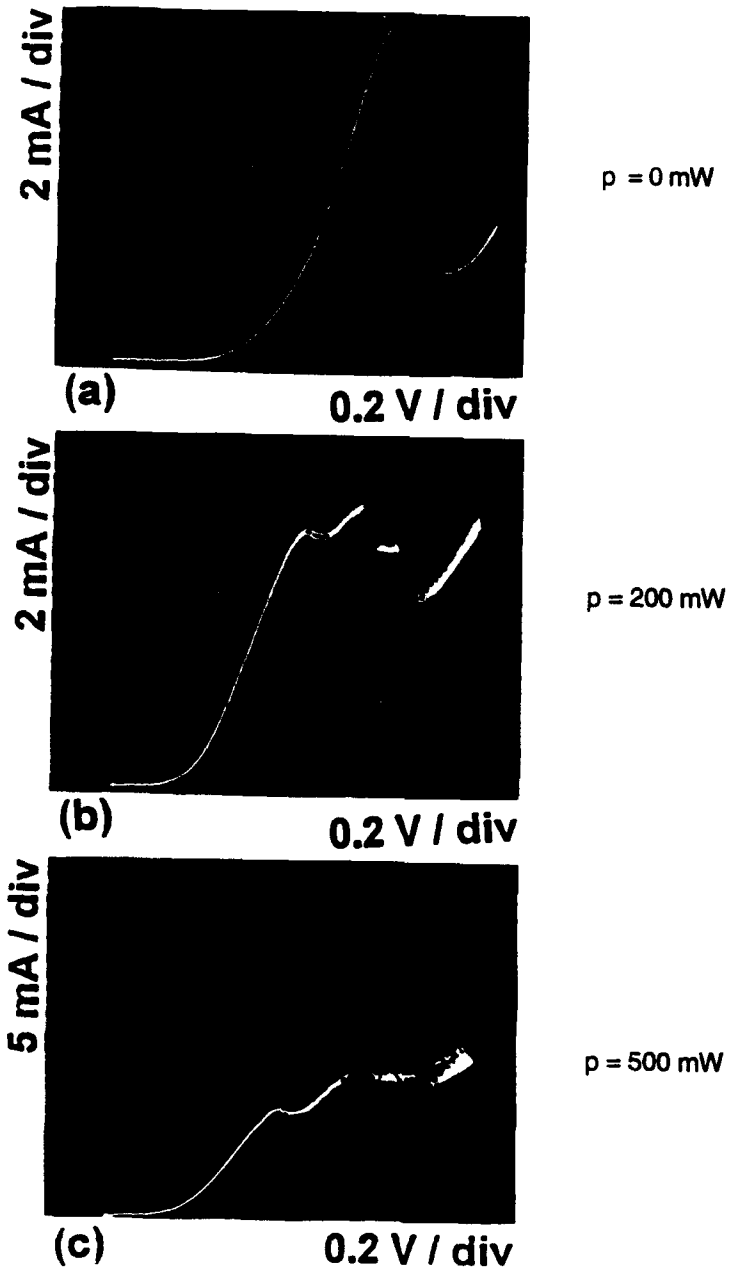

Figure 5-3
I-V Characteristic of Negative Differential Resistance (NDR) in the Resonant Tunneling Diode with Different Illuminating Laser Powers

5.1.2.1 The Working Principle of POC's RTDBQW Optical Switch

In this program, Physical Optics Corporation (POC) has proposed a femtosecond optical guided wave switch/modulator integrated with a resonant tunneling double barrier quantum well (RTDBQW) diode. Figure 5-4 demonstrates a variety of integrated optic modulator/switch configurations in combination with RTDBQW structures. The integrated optic waveguide structures that can be used are: (a) a Mach-Zehnder interferometer modulator; (b) a total internal reflection (TIR) switch; (c) a directional coupling modulator; and (d) a cut-off modulator. The current injection mechanism is performed through the highly efficient RTDBQW with low voltage. The speed of this device is not limited by conventional diode transit times, but only by the quantum tunneling time, which is in the *femtosecond regime* [15]. In addition, *due to its inherent negative resistance current-voltage relationship, the device operates in a bistable mode*. This is an extremely important characteristic if the device is to be used as an optical switch in high performance optical computing systems.

In summary, this structure offers efficient current injection, low switching voltage (~ few volts), super high speed (subpicosecond), and bistable operation. Being the basic building block for super high speed (femtosecond) optoelectronic computing and signal processing, this generic concept has the potential to span a broad variety of unique photonic components, including optical logic gates, EO modulators/switches, variable delay lines, and crossbar reconfigurable interconnects.

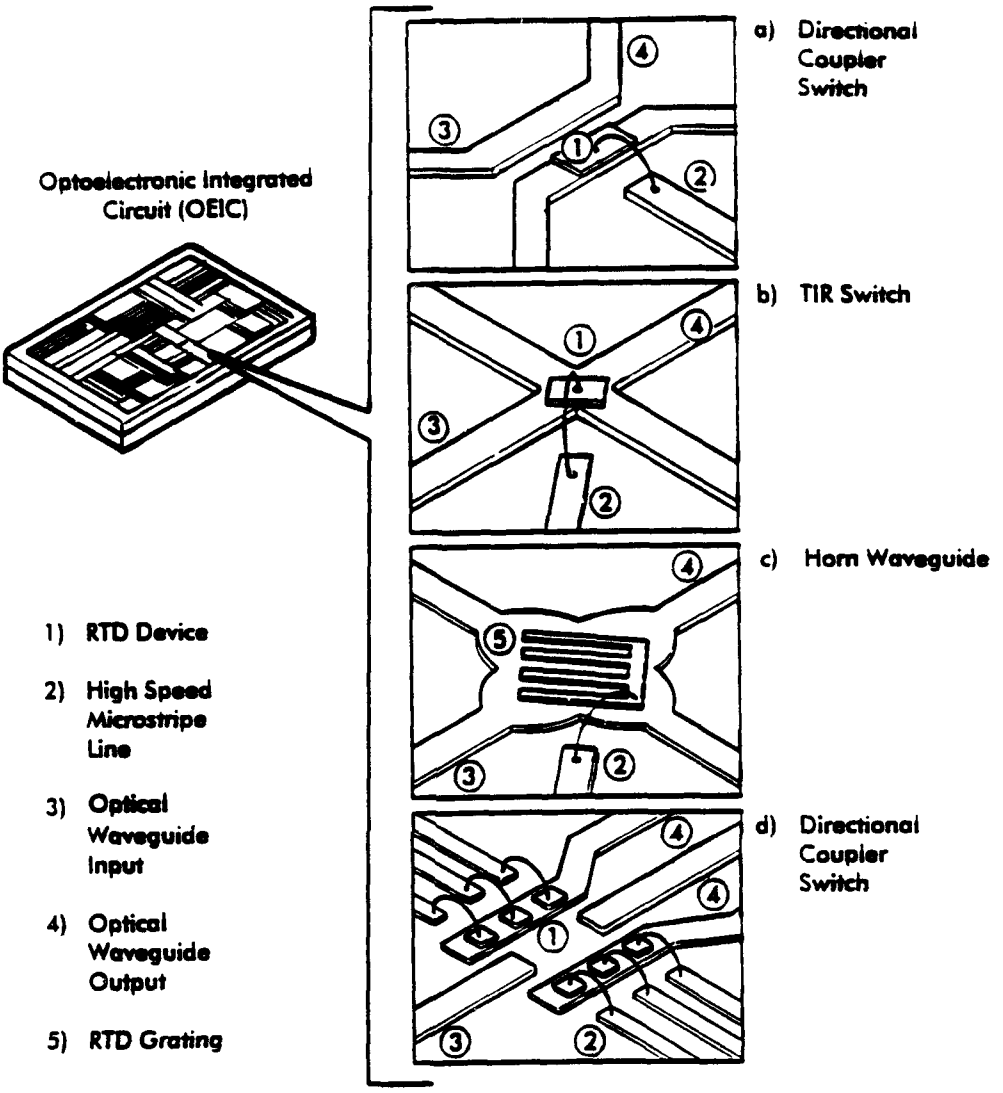

Figure 5-4
POC's Proposed Integrated Modulators/Switches With Resonant Tunneling Double Barrier Quantum Well Diode

6.0 CONCLUSIONS

1. From the achieved all-optical switching results, POC is confident that this Phase II project will end with the successful development of a 10×10 optical crossbar switch. This device represents the next step in state-of-the-art optoelectronics by bridging the gap between integrated optics and semiconductor electronics.

2. The applications for this new technology are far reaching. These applications include: high-speed laser wavelength and incident direction sensors; GaAs-OAM-based IR countermeasure systems; low threshold all-optical crossbar switching devices; delay lines for phased array antennae; optical logic gates; data sampling and encoding; the generation of very short optical pulses; and time division multiplexing (TDM) and demultiplexing. The development of all of these applications will be crucial to the development of super fast optical computers.

3. Due to the large modulation depths achieved (> 85%), as compared to those achievable with EO modulators (which require high driving voltages), the all-optical switch will be a much more efficient and low power device.

4. With POC's unique QW structure designs, the optical switching speed can be enhanced from the nanosecond (limited by carrier lifetime) to picosecond level. This will give much higher modulation speeds than conventional high bias EO modulators.

5. A low cost all-optical switch can be easily achieved, due to the reduction of sophisticated device processing and electronic interconnection.

7.0 REFERENCES

1. R. Chen, "An Optically Activated Modulator and GaAs-GaAlAs Compound Semiconductor Channel Waveguide," Final Report to SDIO, Contract No. F49620-90-C-0068 (1992).

2. R. A. Soref and B. R. Bennett, "Electro-Optic Effects in Silicon," IEEE J. of Quantum Electron., QE-23, 123 (1987).

3. J. P. Lorenzo and R. A. Soref, "1.3 mm Electro-Optic Silicon Switch," Appl. Phys. Lett., 51, 6 (1987).

4. N. K. Dutta, N. A. Olsson, and W. T. Tsang, "Carrier Induced Refractive Index Change in AlGaAs Quantum Well Lasers," Appl. Phys. Lett., 45, 836 (1984).

5. J. Manning, R. Olshansky, and C. B. Su, "Strong Influence of Nonlinear Gain on Spectral and Dynamic Characteristics of InGaAsP Laser," Electron. Lett., 21, 496 (1985).

6. O. Mikami and H. Nakagome, "Waveguide Optical Switch in InGaAs/InP Using Free-Carrier Plasma Dispersion," Electron. Lett., 20, 228 (1984).

7. K. Ishida, H. Nakamura, R. Matsumura, T. Kadoi, and H. Inoue, "InGaAsP/InP Optical Switches Using Carrier Induced Refractive Index Change," Appl. Phys. Lett., 50, 141 (1987).

8. N. W. Ashcroft et al., Solid State Physics (Cornell University, Ithaca, NY, 1976).

9. R. Tsu and L. Esaki, Appl. Phys. Lett., 22 562 (1975).

10. T. C. L. G. Sollner, W. D. Goodhue, P. E. Tannenwald, C. D. Park, and D. D. Peck, IEEE Trans. Electron Devices, ED-30, 1577 (1983).

11. A. Zaslavsky, V. J. Goldman, and D. C. Tasui, "Resonant Tunneling and Intrinsic Bistability in Asymmetric Double-Barrier Heterostructure," Appl. Phys. Lett., 53, 1408 (1988).

12. T. P. E. Broekaert, W. Lee, and C. G. Gunstad, "Pseudomorphic $In_{0.53}Ga_{0.47}$ As/AlAs/InAs Resonant Tunneling Diodes with Peak-to-Valley Current Ratios of 30 at Room Temperature," Appl. Phys. Lett., 53, 1545 (1988).

13. E. Wolak, E. Özbay, B. G. Park, K. Diamond, D. M. Bloom, and J. Harris, "The Design of GaAs/AlAs Resonant Tunneling Diodes with Peak Current Densitites Over 2×10^5 A/cm^2," J. Appl. Phys, 69 3345 (1991).

14. I. Grive, S. C. Kan, G. Griffel, S. W. Wu, A. Sa'ar, and A. Yariv, "Monolithic Integration of a Resonant Tunneling Diode and a Quantum Well Semiconductor Laser," Appl. Phys. Lett., 58 110 (1991).

15. J. F. Whitaker and G. A Mourou, "Picosecond Switching Time Measurement of a Resonant Tunneling Diode," Appl. Phys. Lett., 53 385 (1977).

16. A.E.J. Marcatili, "Dielectric Rectangular Waveguide and Directional Coupler for Integrated Optics," Bell Sys. Tech. J., 48, 2071 (1969).